Pore-level modeling of immiscible drainage: validation in the invasion percolation and DLA limits

M. Ferer[a,b,*], Grant S. Bromhal[c], Duane H. Smith[d,e]

[a] *National Energy Technology Laboratory, Morgantown, WV 26507-0880, USA*
[b] *Department of Physics, West Virginia University, P.O. Box 6315, Morgantown, WV 26506-6315, USA*
[c] *US DOE, National Energy Technology Laboratory, Morgantown, WV 26507-0880, USA*
[d] *US DOE, National Energy Technology Laboratory, Morgantown, WV 26507-0880, USA*
[e] *Department of Physics, West Virginia University, USA*

Abstract

Motivated by a wide-range of applications from ground water remediation to carbon dioxide sequestration and by difficulties in reconciling experiments with previous modeling, we have developed a pore-level model of two-phase flow in porous media. We have attempted to make our model as physical and as reliable as possible, incorporating both capillary effects and viscous effects. After a detailed discussion of the model, we validate it in the very different limits of zero capillary number and zero-viscosity ratio. Invasion percolation (IP) models the flow in the limit of zero capillary number; results from our model show detailed agreement with results from IP, for small capillary numbers. Diffusion limited aggregation (DLA) models the flow in the limit of zero-viscosity ratio; flow patterns from our model have the same fractal dimension as patterns from DLA for small viscosity ratios.
c

Keywords: Pore-level modeling; Immiscible drainage; Invasion percolation; DLA

* Corresponding author. Tel.: +1-304-293-3422; fax: +1-304-293-5732.
E-mail address: mferer@wvu.edu (M. Ferer).

1. Introduction

Flow through porous media is a subject of scientific and engineering interest for a number of reasons, e.g. enhanced oil recovery, DNAPL remediation, and CO_2 sequestration. For half a century, flow in porous media has been treated as a compact (i.e., Euclidean) process whereby the interface advances linearly with the total amount of injected fluid. This behavior is predicted by a Darcy's law treatment, that uses saturation-dependent relative permeabilities, such as those of Buckley–Leverett or Koval [1–5]. In the last 15 years, it has been appreciated that flow in porous media is fractal in certain well-defined limits [6–10]. In the limit of zero-viscosity ratio, $M = \mu_I/\mu_D = 0$ (i.e., ratio of the viscosity of the injected fluid to that of the displaced fluid), the flow is known to be modeled by self-similar, diffusion-limited-aggregation (DLA) fractals. Here, the injected fluid has zero viscosity and the displaced fluid has finite viscosity [6–9,11–13]. The flow is known to be modeled by self-similar, invasion percolation fractals in the limit of zero capillary number, $N_c = \mu_D V/\sigma \cos\theta = 0$, where viscous drag forces (viscosity of the displaced fluid times average fluid velocity, $\mu_D V$) are zero, while the capillary forces (proportional to interfacial tension, σ, times cosine of the contact angle θ) are finite.

In a series of papers, we had studied unstable (viscosity ratio $M < 1$) miscible (zero surface tension) injection using a pore level model similar to Chen and Wilkinson [11], Lenormand [6], and Blunt and King [7]. That is, we performed pore-level modeling of the injection of a less viscous fluid into a model porous medium saturated with a more viscous fluid, with viscosity ratio, $M = \mu_I/\mu_D < 1$, and zero surface tension. We found that initially the fluid injection was described by DLA fractals, but as the fluid advanced, the injection became compact on a time-scale inversely related to the viscosity ratio, M. That is, the smaller the viscosity ratio, the longer it took for the flow behavior to 'cross over' from fractal to compact behavior, so that the only flows that remained fractal were those in the zero-viscosity ratio limit [14–17]. (It should be noted that in this series of earlier papers, the inverse viscosity ratio was used, i.e., $M_{\text{earlier}} = 1/M$.) This crossover was observed in both two- and three-dimensional flow; [14,17] the crossover affected both the saturation of injected fluid and the interfacial width [15,16]. The behavior of this crossover enabled us to characterize the dependencies of saturation and fractional flow upon the viscosity ratio, in the long-time, compact limit to which the assumptions of standard Darcy's law flow are limited.

In Section 2 of this paper, we present a model which includes both viscous and surface tension effects to simulate the injection of an immiscible, non-wetting fluid into a model two-dimensional porous medium saturated with a wetting fluid. In the appropriate limits, our model provides results consistent with DLA and invasion percolation (IP), as discussed in Sections 3 and 4, respectively.

DLA was originally introduced to describe colloidal aggregation [18]. Soon, it was appreciated that because the continuum versions of both DLA and viscous fingering are governed by Laplace's equation, both should provide equivalent displacement patterns in the limit of zero viscosity ratio [19]. Indeed, evidence from both experiments and modeling showed that not only were the DLA and viscous fingering patterns visually similar, but they also had the same fractal dimension [6–10,12–17,20].

Section 3 presents evidence that our two-dimensional modeling for small viscosity ratio and zero interfacial tension produces displacement patterns which have the same fractal character as DLA patterns.

IP was proposed as a model of immiscible drainage (a non-wetting fluid is injected into a medium saturated with a wetting fluid), in the limit of zero injection velocity, i.e., at zero capillary number [8–10,21]. In IP, only the largest throat (with the smallest capillary pressure) on the interface is invaded by the injected, non-wetting fluid.

When using the IP rule, it is assumed that wetting fluid will be displaced towards the outlet. However, in two dimensions, one may need to include trapping effects where a blob of the wetting fluid cannot reach the outlet because it is surrounded by non-wetting fluid. The injected fluid patterns resulting from IP with trapping have been observed to have a fractal character with a fractal dimension $D \approx 1.82$ [8–10,21]. Experiments have produced patterns of two-dimensional drainage at small capillary number ($N_c = 10^{-5}$), which are visually similar to patterns from IPwt and which have the same fractal dimension, $D \approx 1.84$, as IPwt [22]. Section 4 of this paper shows that our model produces saturation profiles and flow patterns which are identical to those from IPwt. We also discuss the deviations from IPwt that arise as capillary number is increased.

Demonstration of the validity of our pore-level model in these two very different limits, coupled with the physicality of the model and the excellent consistency of our results with fluid conservation indicate that the model can be reliably extended to the physically relevant intermediate regime where the limiting models (DLA and IPwt) cease to be valid. To our knowledge, this is the most complete quantitative validation of a member of the class of pore-level models. Even though the validating tests have been performed using results from our model, the other pore level models are similar enough that they may be equally valid, although such extensive, quantitative tests have not been performed for these models [6–11].

2. Description of the model

Our pore-level model is intended to incorporate, as realistically as possible, both the capillary pressure that tends to block the invasion of narrow throats and the viscous pressure drop in a flowing fluid. The two-dimensional porous medium was modeled as a diamond lattice with a length scale ℓ, Fig. 1, which consists of spherical pore-bodies of volume, ℓ^3, $((4\pi/3)r^3 = \ell^3)$ at the lattice sites; connecting these pore-bodies are cylindrical throats which are of length, ℓ, and have a randomly chosen cross-sectional area between 0 and ℓ^2 $(\pi R^2 = 0 \rightarrow \ell^2)$, i.e., there is equal probability for any area between 0 and ℓ^2. Compared to several models reported in the recent literature, we believe that our model should be both more general and more flexible, in part because both the throats and the pore bodies have finite volume in comparison with (i) Refs. [6,23], where the throats contain zero volume of fluid, and (ii) Refs. [24–26], where the pore bodies have zero volume. Furthermore, in our model, the volumes of both the pore bodies and throats can be set as desired. In this sense, the work of Periera

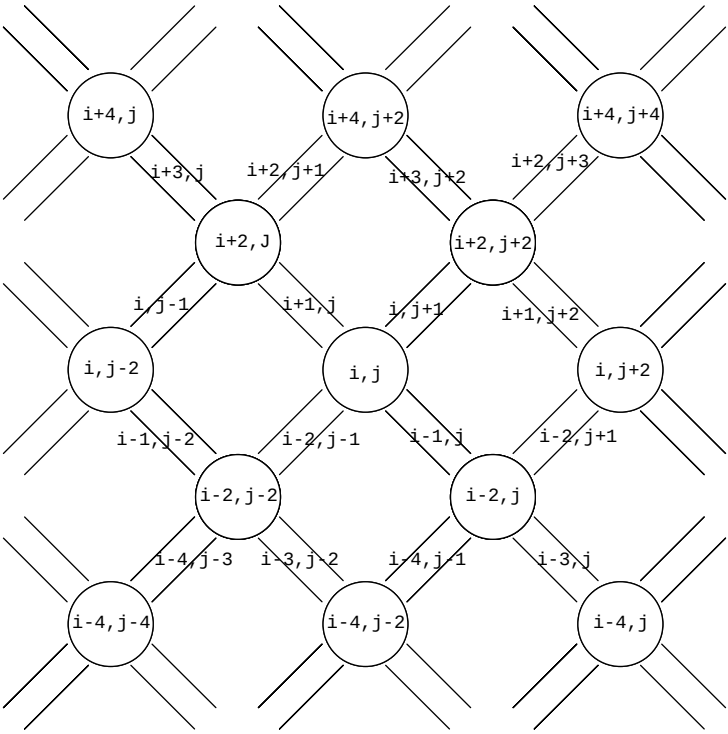

Fig. 1. A portion of the two-dimensional porous medium. The pore bodies, labeled by two even integers, occupy the sites of a diamond lattice. Adjacent pore bodies are connected by pore throats, labeled, as shown, by one even and one odd integer. In this figure, flow is directed upwards, with the inlet being the bottom row of throats, and the outlet being the top. The diamond lattice structure was chosen instead of a square lattice to minimize spurious blocking of throats that are perpendicular to the direction of average flow.

is closer to our model, but the latter work focuses on a model of three-phase flows at constant pressure [27]. Of course all of these models include the essential features of random capillary pressures that block the narrowest throats and a random conductivity that depends on the viscosity ratio.

2.1. *Capillary pressure*

When the invading fluid first enters one of the pore throats, the radius of curvature, R, of the meniscus is fixed by contact angle, θ, and the radius of the pore throat, r;

$$R = r/\cos\theta \ . \tag{1}$$

Therefore, the pressure drop across the meniscus is the capillary pressure

$$P_{\text{cap}}(R) = \frac{2\sigma\cos\theta}{r} \ , \tag{2}$$

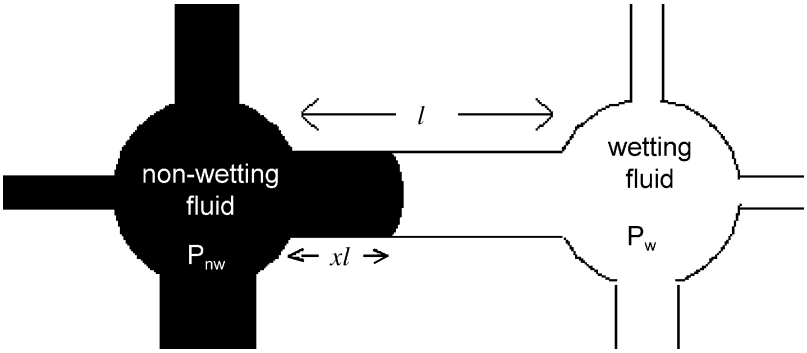

Fig. 2. A sketch showing the advance of the non-wetting fluid within a throat where the pressure drop exceeds the capillary pressure, as given in Eqs. (2)–(4).

where σ is the surface tension. Thus, the flow velocity is given by the throat conductance times the total pressure drop across the throat; see Fig. 2,

$$q = g_{\text{throat}}(P_{\text{nw}} - P_{\text{w}} - P_{\text{cap}}) \, . \tag{3}$$

In the model, the transmissibility (conductance) of the throat is given by Poiseuille's law,

$$g_{\text{throat}} = g^* \frac{(A^2_{\text{throat}}/\ell^4)}{(x + (1-x)M)} \, , \tag{4}$$

where A_{throat} is the cross-sectional area of the throat (randomly chosen from a uniform distribution), x is the fraction of the throat of length ℓ which is filled with defending fluid, and M is the ratio of the non-wetting, invading fluid's viscosity to that of the wetting, defending fluid, $M = \mu_{\text{I}}/\mu_{\text{D}}$. (Note: this definition of M agrees with the convention of Lenormand [6], but it is the inverse of the convention used in our earlier papers on miscible, unstable flow [14–17].) The quantity, g^*, carries all the dimensionality of g_{throat}, $g^* = \ell^3/(8\pi\mu_{\text{w}})$. Many of our results for the flow velocity are presented in terms of $q^* = q/g^*$, which is independent of the particular value of the viscosity of the wetting fluid. From Eq. (3), the non-wetting fluid advances if the pressure difference between the pore filled with non-wetting fluid and the pore filled with wetting fluid exceeds the capillary pressure. Otherwise the non-wetting fluid will retreat.

Naive use of Eq. (2) causes a number of complications in the programming. These complications arise because of the blocking that can occur if the non-wetting fluid is at the entrance to a throat (see Fig. 3); if the sign of the pressure drop $(P_{\text{nw}} - P_{\text{w}})$ is such that it would advance the non-wetting fluid but the magnitude of the pressure drop does not exceed the capillary pressure $(P_{\text{nw}} - P_{\text{w}} < P_{\text{cap}})$, the interface remains stationary at the inlet of the throat. If the non-wetting fluid is close to the entrance of a narrow throat which will likely be blocked to the invading fluid, a very small time step may be required to advance the fluid to the entrance of the throat, but not into the throat. This makes a reliable control of the velocity difficult because a small change in pressure can lead to a large change in velocity if it is large enough to unblock

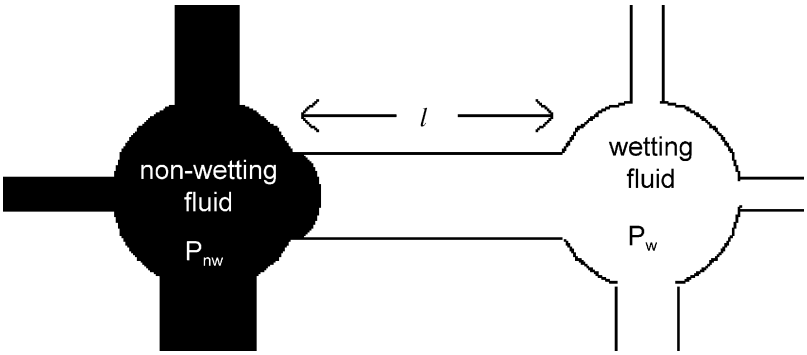

Fig. 3. A sketch showing the blocking that can occur if the non-wetting fluid is at the entrance to a throat while the pressure drop ($P_{nw} - P_w$) is not big enough to advance the meniscus into the throat.

one or more throats. A clever solution to these problems was used in Refs. [24,25]; they argued that real throats would have a gradual decrease in cross-sectional area accompanied by a gradual increase in capillary pressure. Consistent with this work, we assume that the capillary pressure increases from zero at the inlet to a throat of radius r and length ℓ to the value in Eq. (2) at the center of the throat. This dependence is given by the equation

$$P_{cap} = \frac{2\sigma \cos\theta}{r} \sin(\pi x)\,, \tag{5}$$

where x is still the fractional distance along the throat from 0 to 1. Eq. (5) solves the problem of trying to advance a fluid into a blocked throat, because the inlet of a throat will never be blocked since it has zero capillary pressure. Furthermore, the problem involving blockage and inlet pressure is removed, so that the constant velocity condition is easier to satisfy.

We found that the time interval through which the interface was advanced had to be chosen with care. Of course, if the interval is too small, the computer program will be unnecessarily inefficient. However, if the interval is too great, large, spurious oscillations occur in the fluid flow about the true equilibrium. For example, in throat A, (see Fig. 4) too large a time step would cause the fluid to advance too far (to a region with too large a capillary pressure for the pressure drop); at the same time, the fluid in throat B would retreat too far (to a region with too small a capillary pressure for the pressure drop). Therefore, a strong restoring force would be set up; the large capillary pressure in A would push the fluid too far back, while the small capillary pressure in B would pull the fluid too far into the throat.

Implicit in this discussion is the assumption that the pressure within a pore body is uniform. Assuming otherwise would require doing full fluid dynamics using the Navier–Stokes equations. This is inconsistent with the pore-level model approach and, given finite computer resources, this would severely limit the size of the model porous medium. While Eq. (5), etc. are idealizations of the real microscopic behavior, the model incorporates the realistic characteristics of a random distribution of conductances

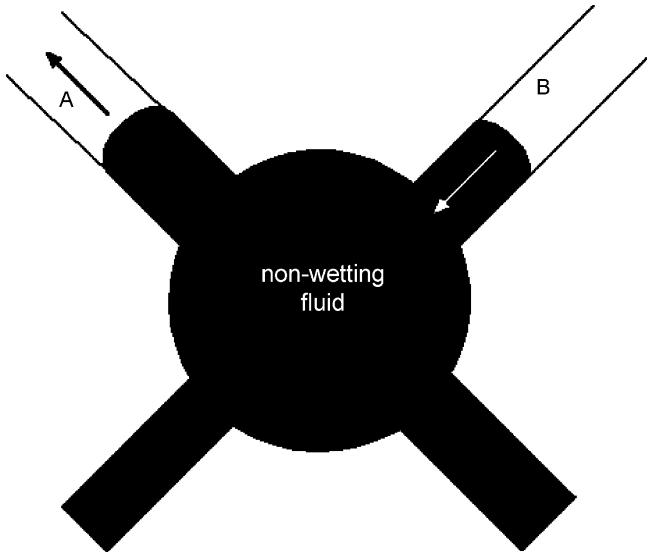

Fig. 4. A sketch showing the oscillations that can occur if the time step is too large. If the time step is too big, the meniscus will advance too far into throat A to a region where the capillary pressure is significantly larger than the pressure drop so that in the next time step there is a large force in the opposite direction on this meniscus. When the meniscus in B moves too far towards the inlet, the capillary pressure decreases too much so that there is a large force in the opposite direction on the meniscus in B.

and correlated capillary pressures. Significantly, the model has the correct dependencies (Eqs. (2)–(4)) upon throat radius for the flow velocity and upon the capillary pressure which must be overcome for the non-wetting fluid to pass through the throat.

2.2. *Finding the pressure field*

Volume conservation of the incompressible fluid dictates that the net volume flow q out of any pore body must be zero. Let us consider application of the above rules to the situations in Fig. 5. In Fig. 5a, the flow velocities directed out of the (i,j) pore body through the throats are

$$q_{i-2,j-1} = g_{i-2,j-1}(P_{i,j} - P_{i-2,j-2}), \quad q_{i,j+1} = g_{i,j+1}(P_{i,j} - P_{i+2,j+2} - P_{\mathrm{cap},i,j+1}),$$
$$q_{i-1,j} = g_{i-1,j}(P_{i,j} - P_{i-2,j} - P_{\mathrm{cap},i-1,j}),$$
$$q_{i+1,j} = g_{i+1,j}(P_{i,j} - P_{i+2,j} - P_{\mathrm{cap},i+1,j}). \tag{6a}$$

Requiring that the net flow out of pore (i,j) be zero leads to the following equation for $P_{i,j}$:

$$(g_{i-2,j-1} + g_{i,j+1} + g_{i-1,j} + g_{i+1,j})P_{i,j}$$
$$= (g_{i-2,j-1}P_{i-2,j-2} + g_{i,j+1}P_{i+2,j+2} + g_{i-1,j}P_{i-2,j} + g_{i+1,j}P_{i+2,j})$$
$$+ (g_{i,j+1}P_{\mathrm{cap},i,j+1} + g_{i-1,j}P_{\mathrm{cap},i-1,j} + g_{i+1,j}P_{\mathrm{cap},i+1,j}). \tag{6b}$$

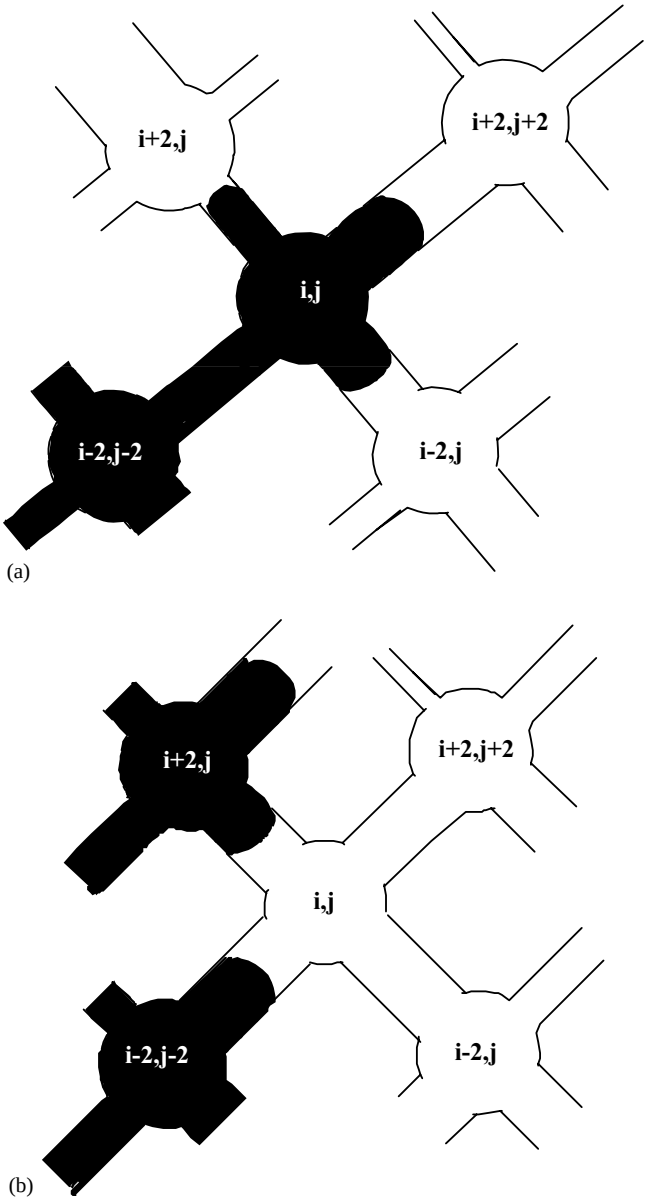

Fig. 5. (a) The fluid occupations near the (i, j) pore giving the flow velocities in Eq. (6), (b) The fluid occupations near the (i, j) pore giving the flow velocities in Eq. (8).

Eq. (6b) is of the general form

$$\left(\sum g\right) P_{i,j} = \left(\sum gP\right) + \left(\sum fgP_{\text{cap}}\right) \ , \tag{7}$$

where (i) the sums are over the connected throats and pore bodies shown in Fig. 5, (ii) the factor f is zero if there is no meniscus in the throat; (iii) the factor f is $+1$ if the pore body (i,j) is filled with non-wetting fluid and the connecting pore body is filled with wetting fluid; (iv) the factor f is -1 if the pore-body (i,j) is filled with wetting fluid and the connecting pore body is filled with non-wetting fluid. For another example, consider the flow velocities in Fig. 5b,

$$q_{i-2,j-1} = g_{i-2,j-1}(P_{i,j} - P_{i-2,j-2} + P_{\text{cap},i-2,j-1}) ,$$

$$q_{i,j+1} = g_{i,j+1}(P_{i,j} - P_{i+2,j+2}) ,$$

$$q_{i-1,j} = g_{i-1,j}(P_{i,j} - P_{i-2,j}), \quad q_{i+1,j} = g_{i+1,j}(P_{i,j} - P_{i+2,j} + P_{\text{cap},i+1,j}) . \tag{8a}$$

Requiring that the net flow out of pore (i,j) be zero leads to the following equation for $P_{i,j}$:

$$\begin{aligned}(g_{i-2,j-1} + g_{i,j+1} + g_{i-1,j} + g_{i+1,j})P_{i,j} \\ = (g_{i-2,j-1}P_{i-2,j-2} + g_{i,j+1}P_{i+2,j+2} + g_{i-1,j}P_{i-2,j} + g_{i+1,j}P_{i+2,j}) \\ +(-g_{i-2,j-1}P_{\text{cap},i-2,j-1} - g_{i+1,j}P_{\text{cap},i+1,j}) .\end{aligned} \tag{8b}$$

Once the location of the interface is known, the numerical value of the capillary pressure in each throat is known (zero, if the interface is neither in the throat nor at either inlet to the throat). Furthermore, for each pore body at (i,j), the values of the sums $(\sum g)$ and $(\sum fgP_{\text{cap}})$ can be calculated and stored; note that these sums are independent of the values of the pressures in the pore bodies. The program then iterates (Eq. (7)), updating the pressure field until convergence is achieved with a residual less than some small value; that is until

$$R = \sum (P_{\text{new}} - P_{\text{old}})^2 < \varepsilon , \tag{9}$$

where ε is chosen to be small, e.g. $\varepsilon = 10^{-3}$. It should be noted that, for the cases being considered, we have used a value of surface tension, so that $2\sigma\cos\theta = 10,000$. Therefore, the smallest pressure drop that will advance the non-wetting fluid through a throat is 17,700, so that our value of the residual represents a fractional pressure change of less than 10^{-11}. This value of ε was chosen to minimize run-time without seriously sacrificing mass conservation. For example, in one of the typical sets of five runs presented in this paper, after an average of 77,000 time steps there was a difference of less than 1% between the total volume of fluid injected into the medium and the total volume of fluid expelled from the medium.

To maintain a constant volume flow q_0, the flow velocity was determined for two estimates of the inlet pressure (the previous inlet pressure $\pm\delta$, typically less than a percent away from the previous inlet pressure). Assuming a linear relationship between flow velocity and inlet pressure (consistent with Eqs. (6a) and (8a)) allows a prediction of an inlet pressure, P_0, used to produce the desired volume flow, q_0 [26]. If the two estimates of the inlet pressure are too close together (δ is too small), the prediction of P_0 will be unreliable; on the other hand, if the estimates of the inlet pressure are too far apart (δ is too big) computer time will be wasted iterating Eq. (7) to

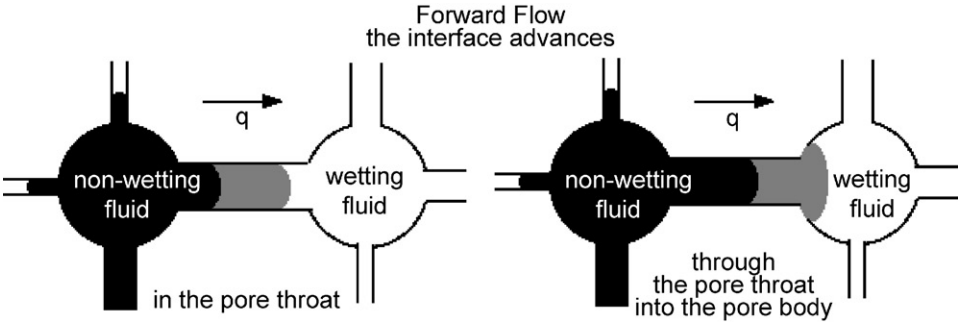

Fig. 6. The flow rules allow the interface to advance (a) within a throat (left side) as well as (b) through a throat into the adjacent pore body (right side).

determine the different pressure fields for each. In practise, the difference between the two initial estimates needs to increase with capillary number. With a good choice of initial estimates, this procedure is very accurate; for a typical set of runs, the coefficient of variation from the average outlet flow velocity, $q = 50.4$, is 0.007%.

2.3. *Flow rules*

Once the pressure field has been determined, the interface can be advanced through a time interval Δt. A throat is considered to be on the interface if the pore body at one end contains some wetting fluid (it may be filled with wetting fluid) and if the pore body at the other end is fully invaded by non-wetting fluid (or was fully invaded and is not yet fully re-invaded by wetting fluid due to backflow). As discussed earlier, a time interval, Δt, needs to be chosen which is small enough that spurious local oscillations in the flow are avoided, but not so small that the program run-time is unnecessarily long. For the cases discussed here with large surface tension, the following prescription seems adequate. For all interfacial throats where the non-wetting fluid has yet to reach the midpoint of that throat (meaning that the capillary pressure is still increasing), the time interval is chosen so that the non-wetting fluid advances no more than 3.5% of the total length into any such throat. For all interfacial throats where the non-wetting fluid has advanced past the midpoint (meaning that the capillary pressure is decreasing), the time step allows the interface to advance no further than 33% of the total length into any such throat. Having determined the interface and chosen the time step, we have attempted to make the flow rules as unrestricted as possible.

Flow can increase the amount of non-wetting fluid within the pore throat (Fig. 6a), or the amount passing through the pore throat into the pore body (Fig. 6b). Similarly, backflow can cause the interface to retreat within the pore throat (Fig. 7a), or through the pore throat into the pore body (Fig. 7b). If, during a time step, either type of fluid overfills a pore body, the excess is shared by the connected outflow throats (those throats with defending fluid flowing out of the pore body). For these flow rules, the

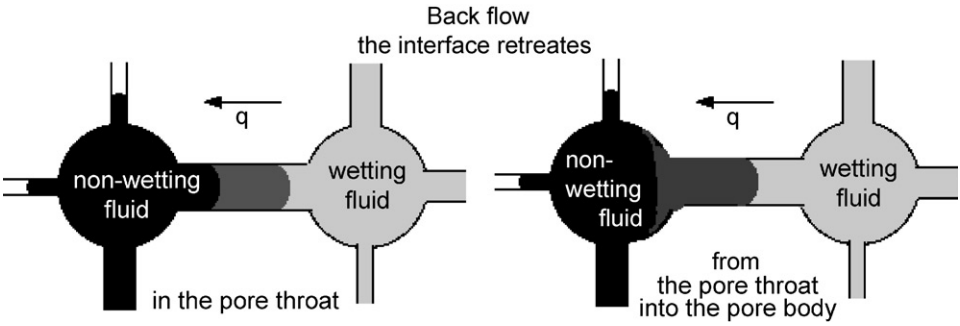

Fig. 7. The flow rules allow the interface to retreat (a) within a throat (left side); as well as (b) through a throat into the adjacent pore body (right side).

throats are taken to be cylindrical with cross-sectional A and length ℓ, consistent with Refs. [24–26,28].

The variation in the capillary pressure along a throat, Eq. (5), might be assumed to result from variations in contact angle, avoiding the problem of having cylindrical throats for volumes and transmissibilities but not for capillary pressure. Again, this aspect of questionable microscopic physicality does not affect the basic feature of the model that the pressure drop across any throat must exceed the capillary pressure of that cylindrical throat, Eq. (2), for the non-wetting fluid to advance through the throat.

Fig. 8 shows a case where the non-wetting (invading) fluid occupies two adjacent pores, without fully occupying the throat between them. The remnant of wetting fluid in the throat will be trapped in the throat unless the pressure drop across the throat is large enough to mobilize the plug of wetting fluid. If the pressure drop across the throat is larger than the capillary pressure, it will push the wetting fluid out of the throat. If this plug of wetting fluid is pushed out of the throat, it will reside in the pore until that pore is fully re-invaded by wetting fluid. Again, this assumption that the wetting fluid will remain in the pore is unphysical because it would be more favorable to have the wetting fluid re-invade the narrower throats filled with non-wetting fluid. The fraction of wetting fluid participating in this unphysical process is determined by the program; fortunately, it was found to be negligible. For the cases considered in this paper, the value of this quantity was zero except for one of the realizations with the largest capillary number, where it represented only 0.07% of the fluid injected. Aspects such as this prevent use of this model to describe imbibition.

If a pore body that was filled with the invading, non-wetting fluid had an influx of the wetting fluid, the build-up of this wetting fluid in the pore body would continue (stored in an imaginary reservoir) with no change of the outflow of non-wetting fluid until the pore body is fully re-invaded by the wetting fluid. This is somewhat unphysical because one would expect the wetting fluid to flow into the narrowest pores filled by non-wetting fluid. The fraction of wetting fluid participating in this unphysical process is calculated in the program, and is not found to be significant (the amount of wetting fluid participating in this unphysical process was less than 1.5% of the total injected fluid).

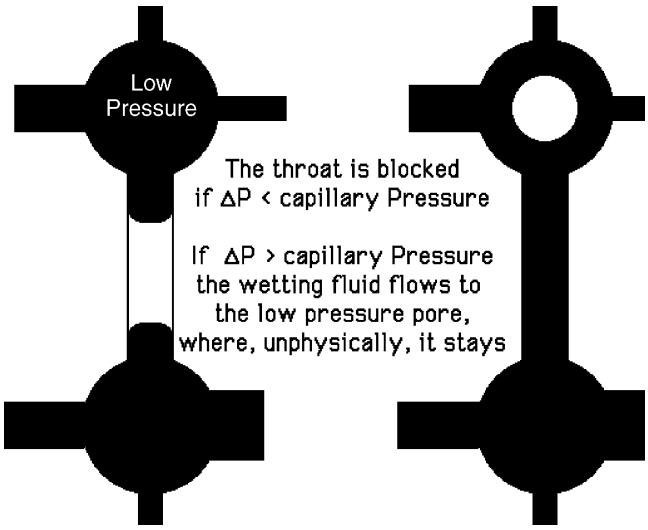

Fig. 8. A plug of wetting fluid which has been 'cut-off' in a throat will remain immobilized (blocking the throat) unless the pressure drop exceeds the capillary pressure in which case the plug is forced into the low pressure pore where the model allows the plug to stay. This unphysical effect of the wetting plug residing in a pore instead of migrating to a narrower throat was found to be negligible in the cases studied.

If the wetting fluid fully re-invades a pore, leaving a plug of non-wetting fluid in a pore throat (see Fig. 9), this plug of non-wetting fluids migrates to the lower-pressure, adjacent pore body, where it is stored in the imaginary reservoir mentioned above. Again, this effect is not found to be significant, representing less than 1% of the total, non-wetting fluid injected.

We have attempted to make the flow rules as non-restrictive and reliable as possible:

(i) All elements of the porous medium (pore throats and pore bodies) have volumes that can be occupied by either type of fluid.
(ii) Locally, back-flow as well as forward-flow are allowed, as ordained by the local pressure differences.
(iii) Complications, such as overfilled pore bodies or plugs of fluid trapped in the pore throats, are treated as physically as possible.
(iv) Unphysical aspects, such as isolated 'blobs' of wetting fluids residing in pore bodies, are tracked by the program and found to be of insignificant magnitude.
(v) Most importantly, the flow rules accurately account for all of the non-wetting fluid injected into the porous medium, from initiation through breakthrough over thousands of time steps. For the smallest capillary number, there is a 0.25% difference between the (a) total volume of non-wetting fluid injected into the medium and (b) the total volume of non-wetting fluid occupying the medium as determined by the flow rules. For the largest capillary number, this difference is less than 0.01%.

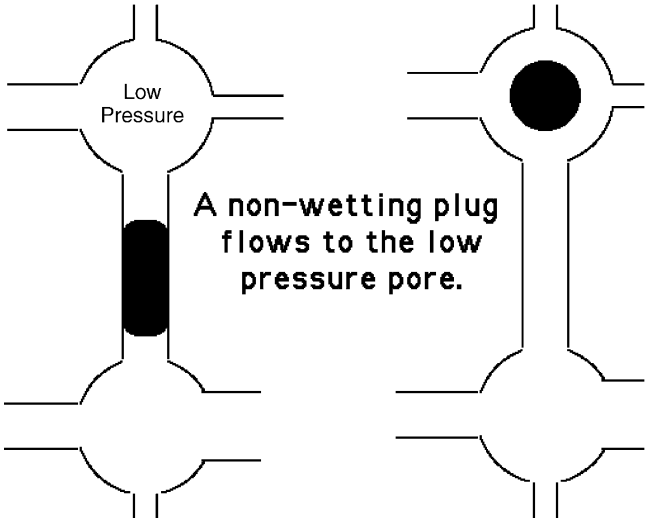

Fig. 9. A plug of non-wetting fluid, which has been 'cut-off' in a throat. This plug will be forced into the lower pressure pore where it stays. In this case, capillary pressure assists in the migration, instead of resisting it as in Fig. 8.

At present, our computer code models the flow in two-dimensional porous media. It should be straightforward to modify our code so that it models flow in three-dimensional porous media; however, computer time considerations will limit this modeling to systems of smaller lateral size than the two-dimensional systems presently under consideration [17].

3. Viscous fingering and diffusion limited aggregation (DLA)

In the limit where viscous fingering dominates, two phase flow in porous media is known to be described by the DLA model [18,19]. Therefore, in the limit of zero capillary pressure (infinite capillary number) and of zero-viscosity ratio, the results from our model should agree with DLA results [6–10,12–17,20].

For central-injection DLA was on a square lattice, the clusters grown were observed to be self-similar fractals with a fractal dimension $D \approx 1.71$ when the clusters occupied approximately $m \approx 10^4$ lattice sites. However, as the size of the cluster increased to more than $m \approx 10^6$ lattice sites, the pattern ceased being self-similar, first becoming diamond shaped and then cross shaped with four distinct arms in the lattice directions [29]. 'Off lattice', mimicking real porous media that lack the symmetry axes of a lattice, the patterns are more self-similar with a fractal dimension $D \approx 1.70$ [30]. Since the DLA simulations on relatively small lattices produce fractal patterns (with approximately 10^4 sites) very similar to very large, off-lattice DLA patterns, we expect that our flow patterns on small diamond-lattice porous media will produce fractal patterns similar to the flow in realistically large, random porous media. In any case, we will compare our flow patterns on small lattices with DLA on similar sized lattices.

To compare our modeling results with DLA, we first developed and ran a program which runs DLA on a diamond lattice with 270,000 lattice sites (300×900). Fig. 10 shows one of the patterns resulting from these simulations; this pattern has approximately $m \approx 20,000$ occupied lattice sites. Given the lattice dependence of DLA, it was important to run DLA on diamond lattices for comparison with model results. Furthermore, because of the size-dependence of on-lattice DLA, we opted to run DLA on diamond lattices, which are almost an order of magnitude larger than the arrays on which the flow model can be efficiently run, so that it would be clear that the self-similar DLA behavior continues to be valid for lattice sizes much larger than can be run on the flow model. Note that the breakdown of self similarity for on-lattice DLA does not set in until the number of occupied sites is a million or more, $m \approx 1,000,000$; two orders of magnitude larger than our DLA simulations. Therefore, for the systems under consideration, on-lattice DLA should be self-similar with a fractal dimension close to that of off-lattice DLA. For purposes of comparison, we ran the flow model to breakthrough for systems with 45,000 pore bodies (150×300), using the following parameter values: viscosity ratio $M = 10^{-4}$ and zero interfacial tension. The model produced DLA-like displacement patterns, with fewer than 10^4 occupied pore bodies (lattice sites), $m \leqslant 10^4$. Given the size of both the DLA and flow-model patterns, one would expect nearly self-similar patterns with a fractal dimension, $D \approx 1.7$, close to that from off-lattice DLA [29,30].

Fig. 11 shows a pattern from the flow model ($M = 10^{-4}$ and zero interfacial tension) in a model porous medium with 30,000 pore bodies (100×300). The fingers from the flow model are somewhat thicker than those from the DLA pattern, otherwise the appearance is quite similar, given the difference in sizes. For a quantitative comparison, Fig. 12 compares the advance of the displacing fluid from our flow model with the advance from DLA. Fig. 12 shows how the average position of the interface $\langle x \rangle$ varies with time; time is proportional to m, the number of lattice sites (or pore bodies) occupied, divided by the width, W; that is, $t = m/W + 0.87$. Both DLA and the flow model indicate that $\langle x \rangle = At^{1/(D-1)}$, where $1/(D-1) = 1 + \varepsilon \approx 1.35$, so that $D \approx 1.74$ is consistent with other DLA results for 'small' clusters; A is a constant called lacunarity. The additive factor 0.87 is a fitting factor which improves the small-t fit to the fractal relation $\langle x \rangle = At^{1/(D-1)}$; the value 0.87 is given by $\frac{1}{2}(2 + \varepsilon)/(1 + \varepsilon)$, determined from modifying the discussion in the appendices of our earlier papers to the present diamond lattice structure [14,16]. As can be seen in Fig. 12, the time is given by m divided by the width for DLA, while it is given by m divided by twice the width for the flow model. This factor of two arises because DLA only occupies the lattice sites (for DLA m equals the number of occupied lattice sites) while the flow model occupies both lattice sites (pore bodies) and pore throats where, on the average, the throats and pore bodies have the same total volume; therefore, in the flow model, m is approximately twice the number of lattice sites occupied. The factor of 1.95 is simply a fitting factor so that the lacunarity ($A \approx 1.17$) is the same for both; in no way does it impact on the value of the exponent. Because the flow model systems are smaller in the flow direction, breakthrough occurs at an earlier t ($t \approx 15$) for the flow model. The larger scatter for the data from the flow modeling results because these systems are smaller in the direction perpendicular to flow (smaller statistical sample). The essential point is

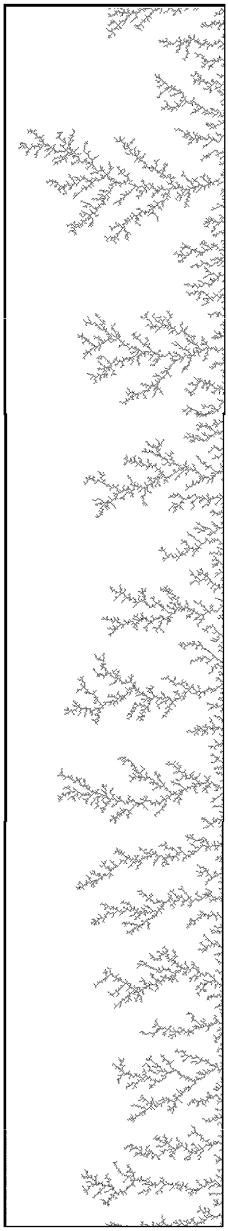

Fig. 10. A typical DLA pattern on a diamond lattice which is 300 lattice sites 'long' by 900 'wide'. In saying the lattice is 300 'long' by 900 'wide', we mean that the i label in Fig. 1 varies from 2×1 to 2×300 and that the label j varies from 2×1 to 2×900. If h is one-half the diagonal (i.e., $h = \ell/\sqrt{2}$), then the lateral dimensions of the figure are 300 h by 1800 h.

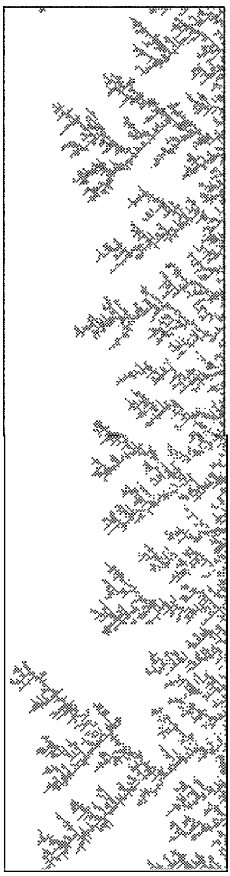

Fig. 11. A typical drainage pattern from the flow model on a lattice which is 150 lattice sites 'long' by 300 'wide'. This pattern is half as long and one-third as wide as the pattern in Fig. 10. However, given the research on size dependence of DLA on lattices, the difference in size between these two patterns is not enough to affect the value of the fractal dimension; i.e., the research on size dependence indicates that DLA patterns of these two sizes should have the same fractal dimension.

that both sets of data have the same functional form. Therefore, the growth of the flow patterns and the DLA patterns are governed by the same value of the fractal dimension ($D = 1.74$), i.e., the same value of the exponent of t ($1 + \varepsilon \approx 1.35$). Therefore, in the limit of zero-viscosity ratio and zero interfacial tension, our model produces results consistent with DLA, as it should.

4. Capillary fingering and invasion percolation (IP)

IP was proposed as a model of immiscible, two-phase flow in porous media in the limit of zero injection velocity, i.e., at zero capillary number [8–10,21]. In IP, each

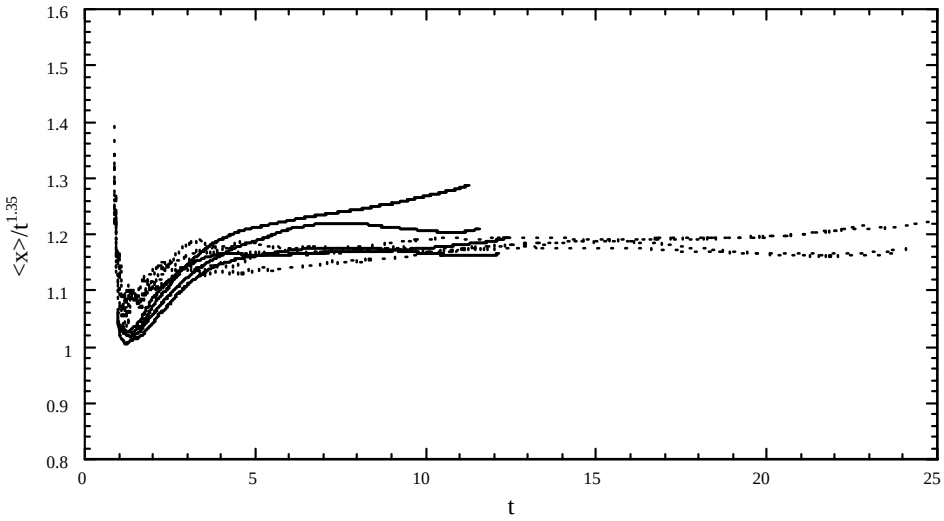

Fig. 12. The scaling ($\langle x\rangle = At^{1/(D-1)}$) of the average position of the interface $\langle x\rangle$ with time $t \approx m/W$ for injection from both DLA (the dashed lines extending to larger times; where $t = (m/900) + 0.87$) and our flow model for $M = 10^{-5}$ (the solid lines ending at $t \approx 12$, where $t = (m/600) + 0.87$). The DLA data has less noise and goes to longer times because the DLA systems are wider and longer, respectively. Because $\langle x\rangle/t^{1.35}$ is constant for both sets of data, the fractal dimension, $D = 1 + (1/1.35)$, is the same for both.

throat in the model porous medium is assigned a random number (in our case, the throat's cross-sectional area). The interface is established at the inlet and advances through that throat having the largest value of the random number. In our case, the throat with the largest cross-sectional area is the throat with the smallest capillary pressure, so that the pressure in the injected, non-wetting fluid is just large enough (equal to the capillary pressure in that largest interfacial throat) to move the fluid through that throat into the adjacent pore body. Having changed the interface, one determines the throat with the smallest capillary pressure on this new interface; the pressure is changed to this value and the injected fluid advances through this throat into the adjacent pore body; and so forth. Note, that unlike our model presented in Section 2, in the IP model the injected fluid can never retreat from a pore once it has invaded that pore.

In this IP rule, it is assumed that wetting fluid will be displaced towards the outlet. However, in two dimensions, trapping effects can be important. The wetting fluid is said to be trapped if the injected, non-wetting fluid surrounds a region of the wetting fluid. That is, if there is a connected path of pore bodies filled with injected fluid, and this path surrounds a region of the wetting fluid, this region of wetting fluid is trapped and cannot be displaced or invaded. If invasion occurred through one of the throats on the perimeter of this region, it would violate fluid conservation because there is no path that the displaced wetting fluid could take to the outlet.

IP with trapping (IPwt) is a modification of the above IP rule in which injected fluid will flow through the pore throat which has both the smallest capillary pressure

and a path to the outlet. Therefore, if there is not a path of wetting fluid from that pore throat to the outlet, the region is trapped and there can be no invasion into that trapped region [8–10,21]. The patterns of injected fluid from IP with trapping have been observed to have a fractal character with a fractal dimension $D \approx 1.82$ [8–10,21]. Experiments have shown that patterns of drainage (injection of a non-wetting fluid into a random porous medium saturated with wetting fluid) at small capillary number ($N_c = 10^{-5}$) have the same fractal dimension, $D \approx 1.84$, as IPwt; and the drainage patterns are visually similar to patterns from IPwt [22].

To test our model near the limit of zero capillary number (where IP is believed to be valid) we have run the model with viscosity ratio $M = 1$ to minimize the effects of viscosity ratio and model parameter $\mathrm{CAPR} = 2\sigma \cos\theta/\ell = 10^4$; for several capillary numbers ranging from $N_c = 1.3 \times 10^{-5}$ to $N_c = 6.4 \times 10^{-3}$ where $N_c = \mu_D V/\sigma \cos\theta$. We present the results for five 900 (30×30) pore-body realizations; five different random number seeds were used to generate five different sets of cross-sectional areas. First, we compare these results with IP results for the same five realizations. Note that we modified the IPwt rules to include the assumed variation of capillary pressure within a throat, Eq. (5). That is, the pressure in the injected fluid was set equal to the pressure necessary to force the injected fluid all the way through the largest radius throat on the interface which was connected to the outlet (not trapped). With this pressure, the other throats on the interface will be invaded to that position x where the capillary pressure in Eq. (5) equals the pressure in the injected fluid. With the above value of the parameters and choosing $q^* = 50$, the capillary number is $N_c = 1.3 \times 10^{-5}$. Fig. 13 shows the near-breakthrough saturation profiles for all five realizations, from both our model and from IPwt. Differences between these saturation profiles for our deterministic model of drainage and for IPwt are negligible, see Figs. 13 and 14. When we compared our model results with results from IP without trapping, IP gave consistently higher saturations at small x where there were more regions of wetting fluid surrounded by non-wetting fluid; the standard IP rule would continue to fill these regions, giving a higher saturation.

An additional comparison is presented in Fig. 14, which compares the patterns from the model and from IPwt for the same five realizations. For realizations #1 and #2, the same pores are invaded in both models, with very few exceptions; this is consistent with the saturation profiles being nearly identical. As with the saturation profiles, there are no significant differences between the results from IP and results from the model with $N_c = 2.6 \times 10^{-6}$.

It is not surprising that finite capillary-number drainage should lead to additional invasion, since the pressures are slightly larger than the minimal capillary pressure of the largest radius throat. If there are interfacial throats with capillary pressures larger than this minimal capillary pressure but smaller than the ‘slightly larger’ pressures in the injected fluid, those interfacial throats will be invaded. Of course, the amount of this extra invasion will increase with capillary number.

Indeed, for larger capillary numbers, the saturation profiles show the typical front of constant saturation moving through the medium, instead of the characteristic fractal profiles where the saturation decreases continuously as the front progresses through the medium (Fig. 14) [31]. Fig. 15 shows the saturation profiles for a range of capillary

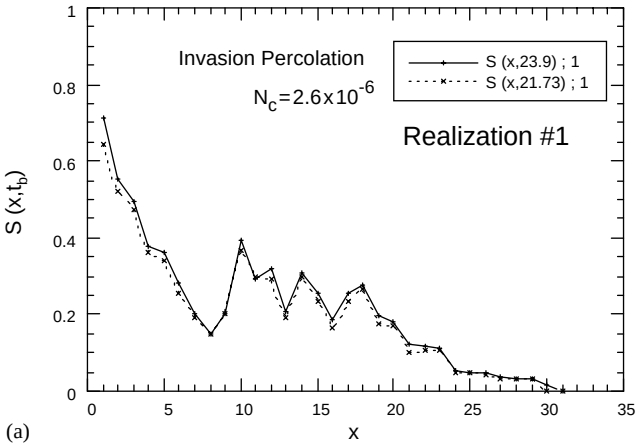

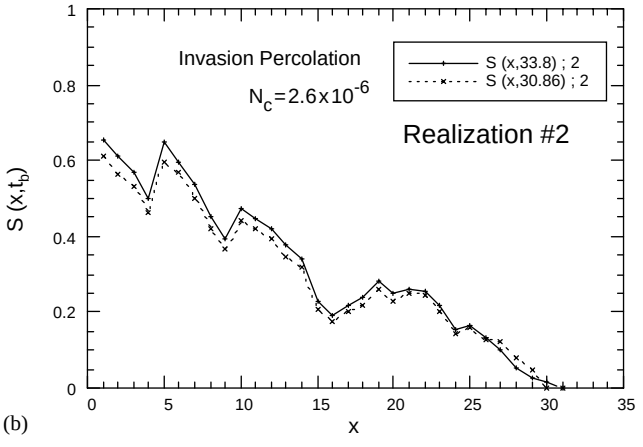

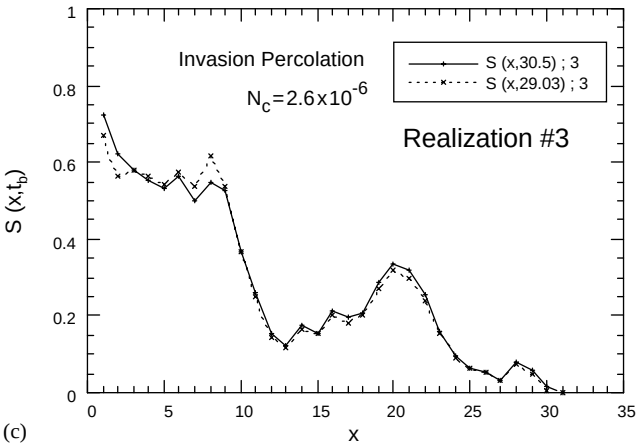

Fig. 13. (a–e) A comparison of the near-breakthrough saturation profiles from the flow model with viscosity ratio $M = 1$ and a small capillary number, $N_c = 2.6 \times 10^{-6}$ with saturation profiles from IPwt for all five realizations. The saturation profiles are nearly the same for both systems for all realizations.

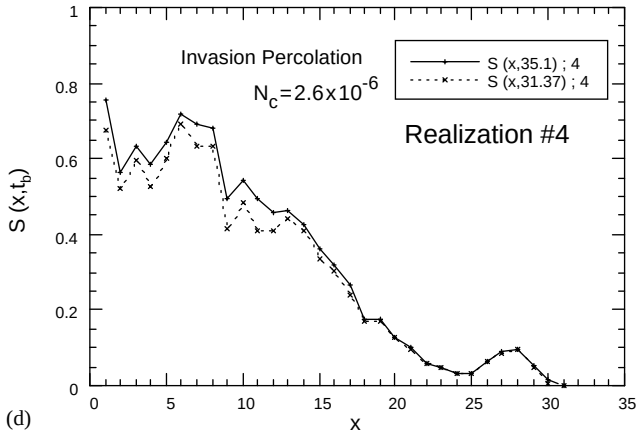

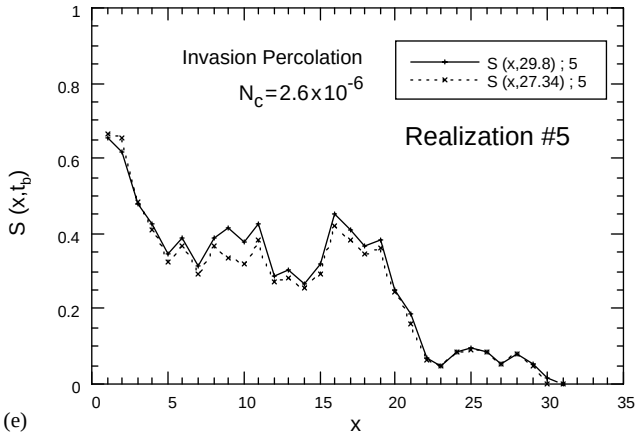

Fig. 13. Continued.

numbers; this clearly shows how the character of the saturation profile changes from a fractal form at small capillary numbers to a conventional Buckley–Leverett form at larger capillary numbers [2,5].

5. Conclusions

We have presented and validated a model of immiscible drainage in porous media. In constructing this model, we have attempted to make it as physical as possible: both in the flow rules as well, as in the relations between the capillary pressures, the conductances, and the geometry of the medium. In cases where there were unphysical aspects in the flow rules, it was determined that they had negligible effect upon results from typical flows. Our model is very similar to several others that have been

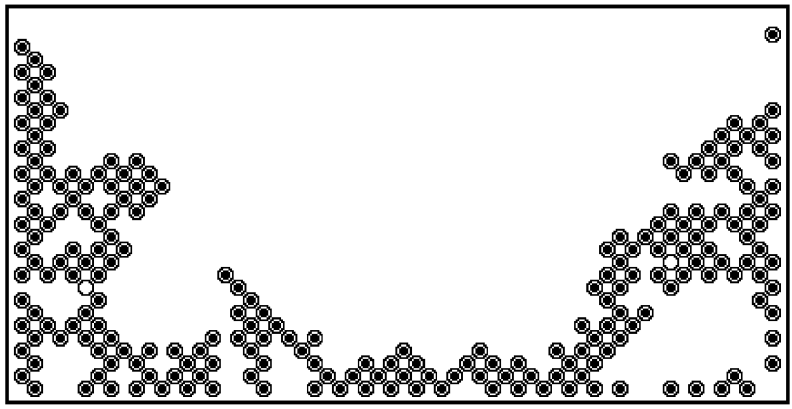

(a)

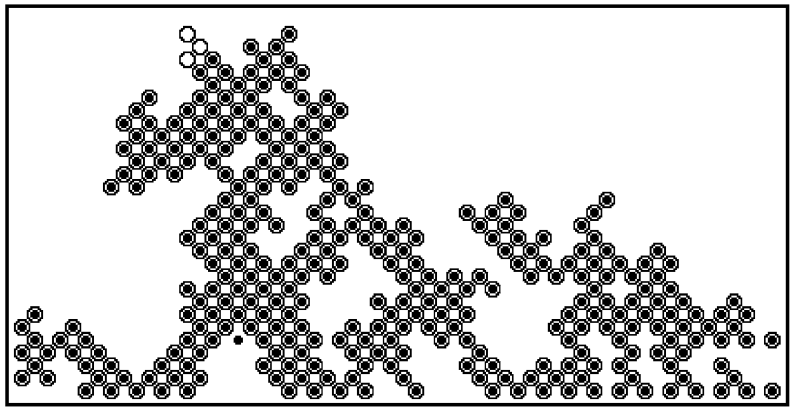

(b)

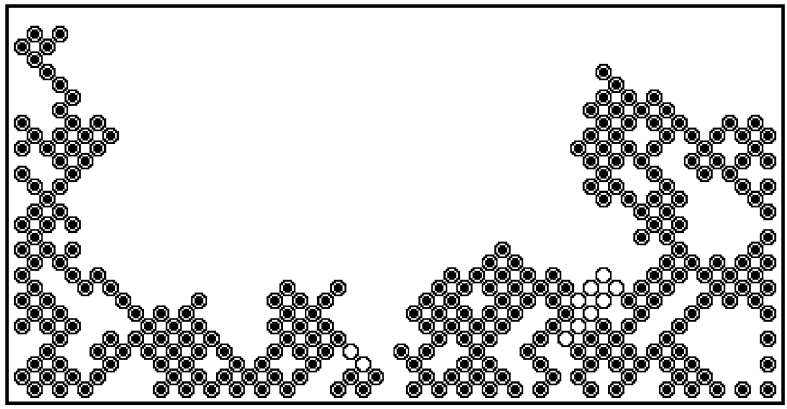

(c)

Fig. 14. (a–e) A comparison of the injection patterns from the flow model with viscosity ratio $M = 1$ and a small capillary number, $N_c = 2.6 \times 10^{-6}$ with injection patterns from IPwt for all five realizations. Pore bodies occupied by non-wetting fluid in the flow model are shown by open circles; those occupied by IPwt are shown by filled circles. Therefore, a filled circle inside an open circle shows that the same pore body was occupied by the flow model and by IPwt during independent simulations. As with saturation profiles, the injection patterns are nearly the same.

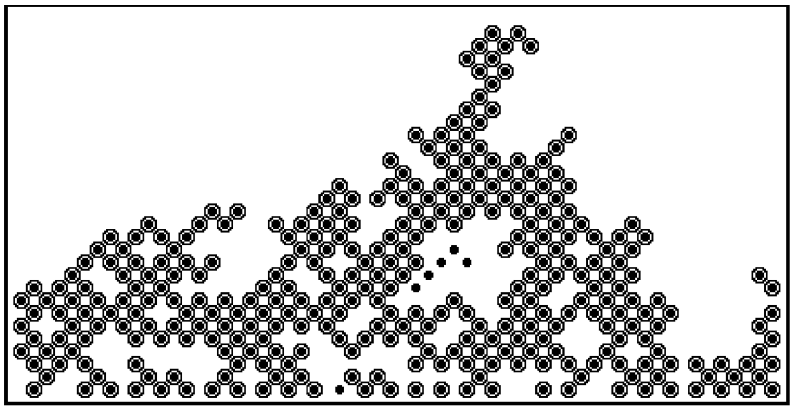

(d)

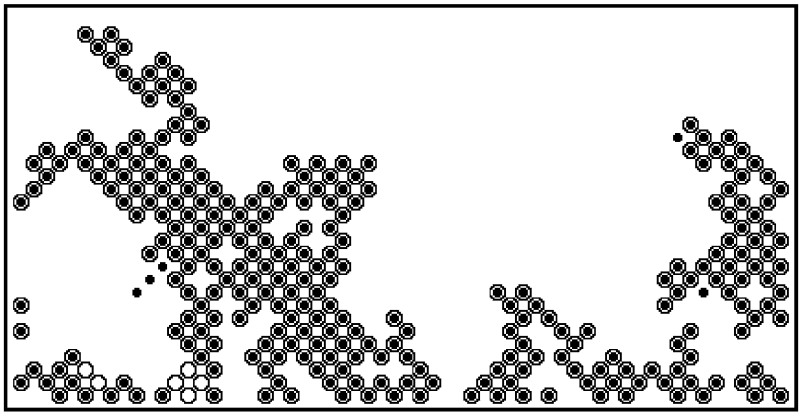

(e)

Fig. 14. Continued.

presented in the literature, but we believe that ours is somewhat more physical and more flexible because both the pore throats and pore bodies have finite (non-zero) volume in our model [6,23–28]. Furthermore, our results are in excellent agreement with fluid conservation; the volume of injected fluid in the medium (as determined by the flow rules), the volume of fluid entering the medium, and the volume of fluid leaving the medium all differ from each other by 1% or less.

We have validated our model in both the small viscosity ratio and small capillary number limits. In the limit of zero-viscosity ratio, the flow is known to produce DLA fractals; for viscosity ratio $M = 10^{-4}$, we have shown that the patterns resulting from our simulations have a fractal dimension indistinguishable from that of DLA on similar-sized lattices. In the limit of zero capillary number, the flow can be modeled by IP with trapping (IPwt). The agreement between results from our small capillary number simulation and IP validates our model in this limit. To our knowledge, this

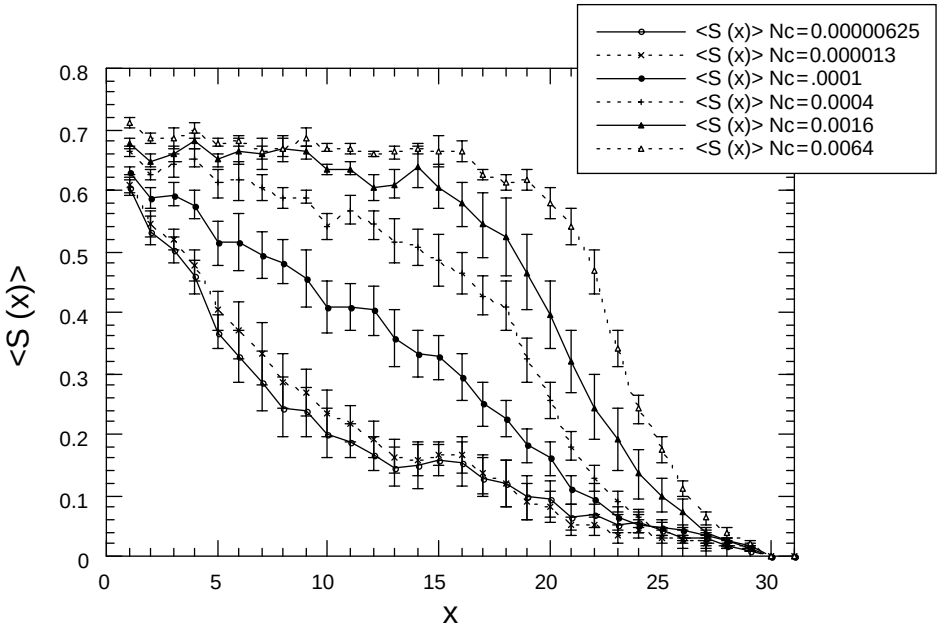

Fig. 15. Near-breakthrough saturation profiles for a range of capillary numbers. The saturation profiles vary from a characteristically fractal form for $N_c \approx 1.3 \times 10^{-5}$, where the saturation decreases throughout the porous medium, to a standard Buckley–Leverett form for $N_c \approx 6.4 \times 10^{-3}$, where the saturation is nearly constant behind the interface and then decreases sharply through the interface.

is the most complete quantitative validation of a member of the class of pore-level models. Even though the validating tests have been performed using results from our model, the other pore level models are similar enough that they may be equally valid, although such extensive, quantitative tests have not been performed for these models [6–11,24–26].

Having validated our model, we can systematically characterize the way that finite capillary number flows deviate from IP, i.e., the way in which the flows crossover from fractal IPwt flows to compact Buckley Leverett flows. Characterizing this crossover should enable us to characterize the dependence of the relative mobilities upon capillary number using methods similar to those in our earlier papers [16,18]. Furthermore, our validated flow model will be used in validating and refining a rule-based model, which is as efficient as DLA or IPwt but whose validity (like the flow model) will span the full parameter space [32].

Acknowledgements

M. Ferer and G. Bromhal gratefully acknowledge the support of the US Department of Energy, Office of Fossil Energy. This work was performed while Grant Bromhal held

a National Research Council Associateship Award at the National Energy Technology Laboratory.

References

[1] R.J. Blackwell, J.R. Rayne, W.M. Terry, Factors influencing the efficiency of miscible displacement, Trans. AIME 216 (1959) 1–8.
[2] R.E. Collins, Flow of Fluids through Porous Materials, Reinhold Publ. Corp., New York, 1961.
[3] J. Bear, Hydraulics of Ground Water, McGraw-Hill Publ. Co., New York, 1979.
[4] F.A.L. Dullien, Porous Media: Fluid Transport and Pore Structure, Academic Press, New York, 1979.
[5] H.-K. Rhee, R. Aris, N.R. Amundson, First—Order Partial Differential Equations, Vol. I (Theory and Applications of Single Equations), Prentice-Hall, Englewood Cliffs, NJ, 1986.
[6] R. Lenormand, E. Touboul, C. Zarcone, Numerical models and experiments on immiscible displacements in porous media, J. Fluid Mech. 189 (1988) 165–187.
[7] M. Blunt, P. King, Relative permeabilities from two- and three-dimensional pore-scale network modeling, Trans. Porous Media 6 (1991) 407–433.
[8] J. Feder, Fractals, Plenum Press, New York, 1988.
[9] T. Vicsek, Fractal Growth Phenomena, World Scientific, Singapore, 1989.
[10] P. Meakin, Fractals, Scaling, and Growth Far From Equilibrium, Cambridge University Press, Cambridge, 1998.
[11] J. Chen, D. Wilkinson, Pore-scale viscous fingering in porous media, Phys. Rev. Lett. 55 (18) (1985) 1892–1895.
[12] J. Nittmann, G. Daccord, H.E. Stanley, Fractal growth of viscous fingers: quantitative characterization of a fluid instability phenomenon, Nature 314 (1985) 141–144.
[13] G. Daccord, J. Nittmann, H.E. Stanley, Radial viscous fingers and diffusion-limited aggregation: fractal dimension and growth sites, Phys. Rev. Lett. 56 (4) (1986) 336.
[14] M. Ferer, R.A. Geisbrecht, W.N. Sams, D.H. Smith, Crossover from fractal to compact growth from simulations of two phase flow with finite viscosity ratio in two-dimensional porous media, Phys. Rev. A 45 (1992) 6973.
[15] M. Ferer, D.H. Smith, Dynamics of growing interfaces from the simulation of unstable flow in random media, Phys. Rev. E 49 (5-A) (1994) 4114–4120.
[16] M. Ferer, W.N. Sams, R.A. Geisbrecht, D.H. Smith, The fractal nature of viscous fingering in two-dimensional pore level models, A.I.Ch.E. J. 49 (1995) 749.
[17] M. Ferer, J.C. Gump, D.H. Smith, Fractal nature of viscous fingering in three-dimensional pore-level models, Phys. Rev. E 53 (3) (1996) 2502–2508.
[18] T.A. Witten, L.M. Sander, Diffusion-limited aggregation: a kinetic critical phenomenon, Phys. Rev. Lett. 47 (1981) 1400–1403.
[19] L. Paterson, Diffusion-limited aggregation and two-fluid displacements in porous media, Phys. Rev. Lett. 52 (18) (1984) 1621–1624.
[20] T.C. Halsey, Diffusion-limited aggregation: a model for pattern formation, Phys. Today 53 (11) (2000) 36–41.
[21] D. Wilkinson, J.F. Willemsen, Invasion percolation: a new form of percolation theory, J. Phys. A 16 (1983) 3365–3376.
[22] K. Maloy, F.J. Boger, T. Jossang, Dynamics and structure of viscous fingers in porous media, in: Pynn, Riste (Eds.), Time Dependent Effects in Disordered Materials, Plenum Press, New York, 1987, pp. 111–138.
[23] S.C. van der Marck, T. Matsura, J. Glas, Viscous and capillary pressures during drainage: network simulations and experiments, Phys. Rev. E 56 (5) (1997) 5675–5687.
[24] E. Aker, K. Jorgen-Maloy, A. Hansen, G. Batrouni, A two-dimensional network simulator for two-phase flow in porous media, Trans. Porous Media 32 (1998) 163–186.
[25] E. Aker, K. Jorgen-Maloy, A. Hansen, Simulating temporal evolution of pressure in two-phase flow in porous media, Phys. Rev. E 58 (2) (1998) 2217–2226.

[26] E. Aker, K. Jorgen-Maloy, A. Hansen, Dynamics of stable viscous displacement in porous media, Phys. Rev. E 61 (3) (2000) 2936–2946.
[27] G. Pereira, Numerical pore-scale modeling of three-phase fluid flow: comparison between simulation and experiment, Phys. Rev. E 59 (4) (1999) 4229–4242.
[28] E. Aker, A simulation for two-phase flow in porous media, Univ. Norway Thesis, 1996.
[29] P. Meakin, R.C. Ball, P. Ramanlal, L.M. Sander, Structure of large two-dimensional square lattice diffusion-limited aggregation: approach to symmetric behavior, Phys. Rev. A 35 (1987) 5233–5239.
[30] P. Meakin, L.M. Sander, Comment on Active zone of growth clusters: diffusion-limited aggregation and the Eden model, Phys. Rev. Lett. 54 (1985) 2053.
[31] M. Ferer, W.N. Sams, R.A. Geisbrecht, D.H. Smith, Scaling of fractal flow, Physica A 177 (1991) 273.
[32] G.S. Bromhal, M. Pantazidou, B. Morel, A rule-based network model of DNAPL infiltration: effects of viscous, capillary, and buoyancy forces, submitted to Water Resources Research.